Box, Walter; Västilä, Kaisa; Järvelä, Juha

Flume investigations using natural-like vegetation with a view on fine sediment processes

Published in:
Proceedings of the 38th IAHR World Congress

DOI:
10.3850/38WC092019-0662

Published: 06/09/2019

Document Version
Publisher's PDF, also known as Version of record

Please cite the original version:
Box, W., Västilä, K., & Järvelä, J. (2019). Flume investigations using natural-like vegetation with a view on fine sediment processes. In *Proceedings of the 38th IAHR World Congress* (pp. 5554-5563). Article 38WC092019-0662 (Proceedings of the IAHR World Congress). International Association for Hydro-Environment Engineering and Research. https://doi.org/10.3850/38WC092019-0662

E-proceedings of the 38th IAHR World Congress
September 1-6, 2019, Panama City, Panama
doi:10.3850/38WC092019-0662

FLUME INVESTIGATIONS USING NATURAL-LIKE VEGETATION WITH A VIEW ON FINE SEDIMENT PROCESSES

WALTER BOX[1], KAISA VÄSTILÄ[2] & JUHA JÄRVELÄ[3]

[1,2,3] Department of Built Environment,
Aalto University, School of Engineering, Espoo, Finland
walter.box@aalto.fi; kaisa.vastila@aalto.fi; juha.jarvela@aalto.fi

ABSTRACT

Quantifying vegetative effects on the flow, suspended sediment concentrations, and sediment transport is complicated by uncertainties associated with the correct conceptualization of flow-vegetation-sediment interactions. The aim of this paper is to investigate the vegetative effects on the flow, the spatially varying sediment transport mechanisms, and sediment fluxes for both the unvegetated and vegetated areas of the channel. Experiments were conducted in a laboratory flume at medium to high bulk flow velocities. Care was taken to reproduce vegetated conditions typical of floodplain flows, where the unvegetated main channel and vegetated floodplain are clearly separated, inducing a strong shear flow. Vegetation was represented by a combination of artificial understory grasses and flexible woody plants. Instantaneous flow velocities were measured by acoustic Doppler velocimetry and suspended sediment concentrations by optical turbidity sensors. The suspended sediment concentration increased for positions closer to the bed in the unvegetated part of the channel. However, in and adjacent to the vegetative areas, the vertical profiles of concentration showed more complex distributions. Based on the paired measurements of the flow and concentration the streamwise sediment fluxes were estimated. In the investigated partly vegetated channel the unit sediment discharge was two to four times higher in the unvegetated part compared to the vegetated part of the channel. Data and findings in the present study provide insight on the vertical and lateral variability of suspended sediment fluxes and are useful for predicting sediment transport in partly vegetated channels.

Keywords: Partly vegetative channel; Flexible vegetation; Suspended sediment; Sediment transport; Sediment flux.

1 INTRODUCTION

In vegetated channels, the flow velocities and turbulence intensities are controlled by the presence of vegetation (Aberle and Järvelä, 2015; Caroppi *et al.*, 2019; Rowinski *et al.*, 2018). Factors such as the patch pattern, spatial distribution and density of the vegetation control the bulk flow velocities, as well as lateral and vertical movements of the flow (Västilä and Järvelä, 2018). Understanding the vegetative effects on the flow and sediment transport is important for accurate predictions of the flow capacity and sediment load.

The influence of the flexible vegetation on suspended sediment (SS) transport, both considering the spatial and temporal variation remains less researched with exception of some examples (Hu *et al.*, 2010; Nepf, 2012; Yager and Schmeeckle, 2013). For example, the increased turbulence intensities cause particles to remain in suspension, where otherwise settling would have occurred (Tinoco and Coco, 2018; Yang and Nepf, 2018). The foliation, vegetation density and structure is expected to influence the sediment transport mechanisms and processes as result of secondary flow structures and increased turbulence. Conventionally, vegetation elements have been modelled as rigid elements in both physical flume experiments and models e.g., (Dupuis *et al.*, 2017; Zong and Nepf, 2010, 2011). Increasingly, more research is done on the effects on the flow field and turbulent flow field induced by flexible vegetation with more complex structures and density distributions, ranging from leaf to reach-scale (Elliott *et al.*, 2019; Hu *et al.*, 2018; Vargas-Luna *et al.*, 2016; Västilä and Järvelä, 2018).

In the present study we carefully re-constructed a partly vegetated channel, typical for natural lowland channels during flood conditions with a relatively steep bed (0.15-0.33%) with medium to high bulk flow velocities (0.2-1.2 m/s) and presence of fine sands. The instantaneous flow velocity measurements are paired with concentration measurements allowing the quantification of the suspended sediment fluxes for various regions of the flow, e.g.,(Nikora and Goring, 2002; Ogston and Stenberg, 1995; Shah-Fairbank and Julien, 2016). Consequently, the instantaneous sediment fluxes and the unit sediment discharges can be estimated (Shah-Fairbank and Julien, 2016). This allows us to compare the unit sediment discharges for different lateral positions and compare sediment fluxes between the vegetated and unvegetated areas. Suspended sediment concentrations (SSC) can be measured with high-temporal resolution, and good spatial resolution by optical turbidity sensors (OBS) (Box *et al.*, 2018; Downing, 2006; Tinoco and Coco, 2018). Vertical and lateral

distributions of the concentrations have been measured with good accuracy using OBS's, providing a well-known calibration between the 'true' sediment concentration (mg/l) and optical sensor-response (V).

In the present experiments sediments were transported both as suspended-load and as bed-load. Most of the particles were expected to move in suspension. The bed-load component can be quantified by using e.g., bed-load trappers, bed-load samplers, or image-based particle tracking methods (Gaudet *et al.*, 1994; Yager and Schmeeckle, 2013). In this study, we introduce a downscaled Helley-Smith type bed-load sampler that provides means to measure the near bed sediment fluxes.

The purpose of this study is to investigate the effect of vegetation on the mean flow, the suspended sediment concentration for both the unvegetated part (UP) and vegetated part (VP) of the channel, considering three different vegetated conditions and two flow rates (50 l/s and 83 l/s).

The objectives of this study were to:

i. Quantify the vertical variation in the temporally-averaged streamwise velocity and suspended sediment concentration for the different parts of a partly vegetated channel.
ii. Determine the influence of the bulk flow velocity and the presence of foliage on the suspended sediment fluxes, and unit sediment discharge considering the unvegetated and vegetated parts of the flow.
iii. Develop methodologies capable of determining the suspended load and bed-load components in a vegetated flow considering the challenges arising from scaled laboratory flume applications.

2 METHODS AND LABORATORY CONDITIONS

2.1 Hydraulic conditions

Measurements related to this study were conducted at the Aalto Environmental Hydraulics Lab in the Environmental Hydraulics Flow Channel of 20 m length and 60 cm width, a schematic cross-sectional view is shown in Figure 1. We tested six hydraulic conditions consisting of three vegetated conditions and two flow rates with corresponding discharges of 50 l/s (MQ) and 83 l/s (HQ) (Table 1). The height of the weir, located at the end of the channel, and the slope S_0 of the tilting flume was changed to establish steady quasi-uniform flow conditions of 17 cm depth (h) for all tested conditions. The sediment feeding rate and the duration of the experimental runs were designed so to obtain measurable and natural-like conditions of suspended sediment concentration in both the UP and VP of the channel.

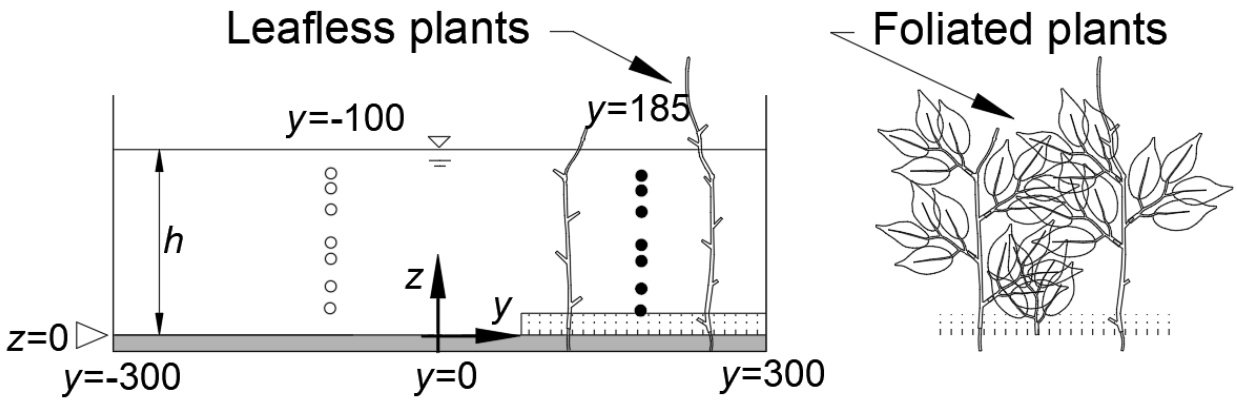

Figure 1. a) Schematic cross-sectional view of the flow channel with representation of the leafless (left) and foliated (right) experimental condition (MQ-L), the understory grasses (dotted area), location of velocity and concentration measurements (circles). The coordinate system unit is millimeters.

2.2 Vegetated conditions

A vegetated patch of 10 m length and 0.23 m of width (located between $70 < y < 300$ mm) was constructed starting 4 m downstream of the flume inlet (D = 0 m, where D is the distance (m) from the start of the vegetated patch). The bed of the vegetative area consisted of dense understory grasses with a height of 20 mm (Figure 1). Three vegetated conditions were tested; dense understory grasses (G), grasses and nearly submerged leafless plants (L), and grasses and nearly submerged foliated plants (F), listed in Table 1. The flexible stems of the just submerged plants were placed in a staggered pattern and had a diameter of 3 mm, and were 205 to 270 mm tall. The frontal projected stem area and one-sided leaf area per unit water volume were 0.11 and 4.1 m^{-1} for the leafless plants and foliated plants, respectively.

Table 1. Experimental conditions: showing the vegetated conditions, discharge Q (l/s), bed-slope S_0 (%), Rouse number *Ro* (-) defined as: $Ro = w_s/\kappa u_x$ $(at\ y = -150\ mm)$, and depth-averaged flow velocities $\bar{u}_{UP}$ and $\bar{u}_{VP}$ (m/s) at *D* = 7 m for the unvegetated and vegetated part of the channel, respectively.

Experimental condition	Vegetated conditions	Q (l/s)	S_o (%)	*Ro* (-)	$\bar{u}_{UP}$ (m/s)	$\bar{u}_{VP}$ (m/s)
1. MQ-G	understory grasses	50	0.15	1.15	0.55	0.41
2. HQ-G	understory grasses	83	0.29	0.74	0.89	0.67
3. MQ-L	grasses & leafless plants	50	0.17	1.02	0.62	0.32
4. HQ-L	grasses & leafless plants	83	0.34	0.59	1.05	0.53
5. MQ-F	grasses & foliated plants	50	0.41	0.83	0.73	0.22
6. HQ-F	grasses & foliated plants	83	0.71	0.54	1.18	0.40

2.3 Velocity measurements

The flow was measured by a Nortek Vectrino plus based on Acoustic Doppler velocimetry (ADV). The presented velocity data in the present paper are composed of existing data (Caroppi *et al.*, 2019) and newly obtained measurements. The point measurements were collected over a duration of 120 s with 200 Hz. The raw ADV data was filtered using a lower limit of the signal to noise ratio (SNR > 15) and a Modified Phase-Space Thresholding despiking algorithm, replacing spikes in velocity with the last good value (Jesson *et al.*, 2015; Parsheh *et al.*, 2010). Statistical averages of the streamwise flow velocity u_x were calculated after filtering of the data. The mean depth averaged-flow velocities $\bar{u}$ were calculated by integration of the measurement points over the vertical assuming the measured u_x located closest to the surface was representative of the surface region. For the unvegetated part of the channel, we integrated from the lowest measurement point (z/h=0.15) to the surface (z/h =1). For the vegetated part, we assumed u_x = 0 in the understory grasses ($z/h \leq$ 0.12) based on results of Caroppi et al. (2019), and integrated from z/h=0 to z/h=1.

2.4 Suspended sediment concentrations

Fine silica quartz sand (Sibelco S90; d_{50} = 150 µm, d_{10} = 110 µm, d_{90} = 190 µm) was selected to avoid cohesive behavior between individual particles ensuring uniform grain-size distribution throughout the experimental runs. The particles had a solid density, ρ_p of 2.65 g/cm^3 and dry bulk density ρ_d of 1.4 g/cm^3. The particles were flat-to-angular shaped, which is typical for natural silica quartz sand. Approximate settling velocities w_s were calculated using the Stokes's law and using the particle drag coefficient as correction for the particle shape. The particle drag coefficient is dependent on the particle Reynolds number Re_p, which is a function of the Shape factor (Julien, 2010). The particle drag coefficient $C_{D,p}$ has been estimated using an iterative approach based on the particle fall velocity w_s and Re_p with a Corey shape factor of 0.7. The approximate settling velocities for the d_{10}, d_{50} and d_{90} were; w_{s10} = 12.4, w_{s50} = 17.2, and w_{s90} = 19.5 mm/s, respectively. The sediments were fed into the channel as a line source upstream of the vegetation at *D* = -2.2 m to support lateral and vertical mixing over the cross-section. The sediments were equally distributed over the flume width by a conical shaped smooth plate and dropped into the water from a height of 10 cm above the water surface. The feeding rate (2.3 g/s) was constant and controlled by an industrially used screw-rotation based feeding system. Sediments reaching flume tank were recirculated back into the inlet by use of a specific designed sediment pump.

Three Campbell Scientific OBS-3+ optical backscatter sensors (OBS) were used to measure the backscattered infrared light intensity in voltage (V) as a measure of suspended sediment concentration with a rate of 10 Hz. The raw voltages were linearly scaled to get an approximate of the suspended sediment concentration in mg/l based on calibration curves obtained for each of the sensors. The calibration curves were established by filtration of manually taken water samples in flume conditions of similar flow velocities, air bubbles, lighting, temperature and particle size distributions. The sensors have a manufacturer-stated accuracy of 4% of the total concentration or 10 mg/l for concentrations less than 250 mg/l. The OBS with the optics facing the upstream flow direction were placed so that most protrusions of the sampling volume, e.g., by the flume boundaries or plant elements were avoided. One-minute point measurements with a rate of 10 Hz were taken for point over the vertical (z = 25, 45, 70, 85, 115 and 135 mm, see Figure 1) in the fully developed region of the flow at *D* = 7 m. The reference concentration C_0 (t) was recorded continuously over the duration of the experimental run at *D* = -1 m in the middle of the flume (y = 0 mm), and at a relative depth of 0.6 h. To allow direct comparisons between individual measurements, the point measurements over the vertical profiles were scaled by the initial reference concentration, C_0 (t = 0) at the start of each experimental run.

Factors that affected the reliability of the concentration measurements are listed in Table 2. This table gives an indication of the sources of the uncertainties and the expected response in relation to the source. In general larger uncertainties were obtained in conditions of low concentrations (approx. < 50 mg/l) due to the increase in the size of the sampling volume, and increase in probability of protrusion of the sampling volume. The total uncertainty, $U(i) = sqrt([u_I^2(i) + u_{II}^2(i)])$ in mg/l for each measurement point, *i* has been estimated based on the standard deviation between two replicate measurements (I) and propagated with the estimated uncertainty from a sensitivity analyses (II) on the calibration curve used. The estimated uncertainties ranged between 1 - 63% and was generally highest for measurements locations where absolute concentrations were less than 50 mg/l and for positions close to the bed ($z/h \leq 0.25$) where very high concentrations were observed. Measurements collected with large uncertainties were discarded from further analyses and left out in the presented figures. In between the experimental runs multiple manual calibrations were conducted, which provided means to validate the used calibration curves. Small differences in the proportion of very fine particles (< 0.063 mm) fed in the experimental runs, which have a larger effect on the turbidity complicated the estimation of the 'real' concentration. However, the initial concentrations were relatively low (approx. 10-20 mg/l) and differences were considered negligible as a result of carefully removing sediments from the flume channel, pipes and tanks after each experimental run.

Table 2. List of factors expected to affect the reliability of the concentration measurements by OBS.

Factors affecting the reliability	Sources of uncertainties
1. Sensor properties	• Sensor sensitivity on particle size and shape, which decreases for larger sized particles. • Intrusion on the flow by the sensor which is dependent on the sensor size and shape. • Disturbance of the sampling volume by the flume boundaries and plant elements, which is larger in conditions of low concentrations due to increasing size of the sampling volume.
2. Environmental conditions	• Temperature affects the sensor response and hydraulic conditions. • Effects of air bubbles which interfere with the sensor-response. • Effects of changes in light intensity. • Effects of dissolved chemicals.
3. Calibration between the sensor output (V) and 'true' suspended sediment concentration (determined from manually taken water samples and filtration and weighting after drying)	• Differences in the in-flume calibration conditions by changes in the sediment feeding rate, particle size and shape distribution. • Non-uniform distribution of the sediment concentration over the flume, resulting in spatial differences between the 'true' SSC and optically measured SSC (OBS sensor). • Temporal differences between the 'true' SSC and the SSC by the OBS sensor. • Changes in background turbidity due to accumulation of very fine sediments and chemicals.

2.4.4 Suspended sediment fluxes

The velocity and concentration measurements were paired based on their spatial position to calculate the SS fluxes q_m and unit sediment discharges q_{tm}. The sediment fluxes q_m (mg $s^{-1}m^{-2}$) were calculated by multiplying the streamwise velocity u_x by the concentration as in:

$$q_m = C_i u_{x,i} \quad [1]$$

Where C_i is the measured SS concentration in mg/l for each point measurement, *i* and $u_{x,i}$ the corresponding average streamwise velocity. The sediment fluxes were integrated over depth to calculate the unit sediment discharge q_{tm} (g $m\text{-}s^{-1}$) similar to (Shah-Fairbank and Julien, 2016):

$$q_{tm} = \sum_0^p \frac{1}{2}(C_i u_{x,i} + C_{i+1} u_{x,i+1})(h_{i+1} - h_i) \quad [2]$$

Where *p* is the number of points over the vertical, $u_{x,i}$ and C_i are the streamwise velocity and SSC at given point *i*, and h_{i+1}-h_i is the vertical layer thickness between the point measurements, respectively.

2.5 Bed-load transport

Direct measurements of the concentration by OBS's at the near bed are complicated due to bed reflections and sensor range. Furthermore, making assumptions on the shape of the vertical concentration profile in the near bed region likely leads to erroneous results. In this study we designed two downscaled Helley-Smith bed-load samplers of rectangular inlet size of 2 by 2 cm (a), and 3 by 3 cm (b) (Figure 2) to obtain the near bed sediment fluxes in future experiments. The samplers were scaled with ratio 1:3.8 (a), and 1:2.6 (b) from an existing Helley-Smith bed-load sampler optimally designed to minimize effects on the flow field (Druffel *et al.*, 1976). The samplers were 3D-printed by a Lulzbot mini 3d printer with 0.5 mm resolution and made of polylactide (PLA), which resulted in hydraulically smooth surfaces of the side walls. The bottom wall at the inlet was sharpened to ease movement of particles at the bed into the sampler, avoiding blockage of the bed-load. The surface area of the sampling bag (mesh size of 35 µm) was large enough to allow filling of the bag while avoiding blockage of the flow (see Figure 2).

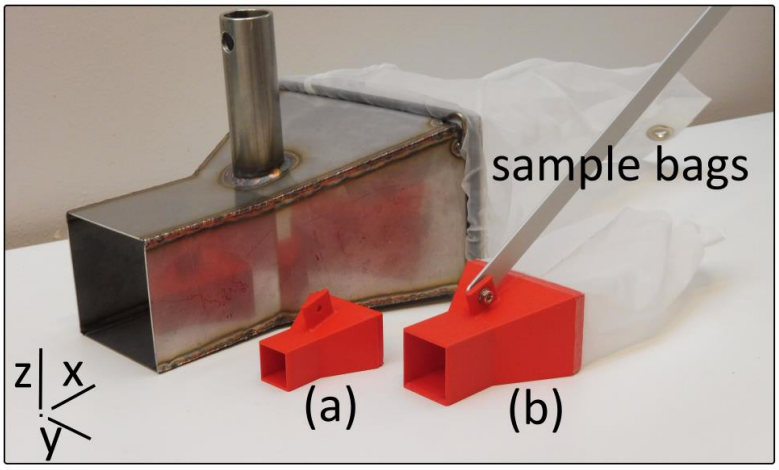

Figure 2. Helley-Smith bed-load sampler (metallic) and the two downscaled bed-load samplers of 2 by 2 cm (a) and 3 by 3 cm (b) (red colored) fabricated by 3D-printing, and sampling bags (white colored). The coordinate system with axis lines x, y and z of 30 mm length is shown to indicate the dimensions.

The downscaled bed-load samplers worked reasonable well based on preliminary tests using the samplers on a smooth PVC bed. Measurements were conducted with good repeatability, the covariance ranged between roughly 5 and 20% for measurements of six repetitions. However, the effects on the flow field induced by the sampler, and flow separation inside the sampler remains unknown. Further test are needed to investigate the sampling efficiency which is expected a function of particle size, bulk flow velocity and turbulence intensity (Gaudet *et al.*, 1994).

4 RESULTS

4.1 Vertical profiles of the time-averaged streamwise velocity

Vertical profiles of the time-averaged streamwise velocity u_x, representing the fully developed flow region at D = 7 m are shown in Figure 3. This figure allow us to compare vertical velocity distributions between the experimental conditions, and point out the effects of the vegetation. The two vertical profiles taken over the cross-section represent the unvegetated part (UP) at y = -100 mm (MQ-G, HQ-G) or y = -150 mm (MQ-L, MQ-F & HQ-L, HQ-F), and the vegetated part (VP) at y = 185 mm (MQ-G, HQ-G) or y = 130 mm (MQ-L, MQ-F & HQ-L, HQ-F) of the channel. In the VP of the channel the depth-averaged flow velocity $\bar{u}_{UP}$ ranged between 0.55 - 1.18 m/s for the tested experimental conditions (Table 1). In the VP of the channel the depth-averaged flow velocity $\bar{u}_{VP}$ ranged between 0.22 - 0.67 m/s. In the fully developed region $\bar{u}$ was 25-71% higher in the UP of the channel compared to the VP as result of the blockage and vegetative drag caused by the vegetation.

In the UP of the channel u_x increased with depth up to a relative depth of 0.6 z/h. For positions larger than 0.6 z/h the velocity profile was more uniformly distributed. A small velocity dip at the surface was observed in the vegetation conditions with understory grasses (G). This was likely the result of the effects of the side walls on the flow field. In the vegetated areas the velocity was close to zero in the understory grasses ($z/h \leq 0.12$) (points not shown in Figure 3), and u_x increased with flow depth between the understory grasses and water surface ($0.12 < z/h < 0.8$). For the high flow rate cases the increase in u_x over depth was considerable stronger compared to in the low flow rate (Figure 3).

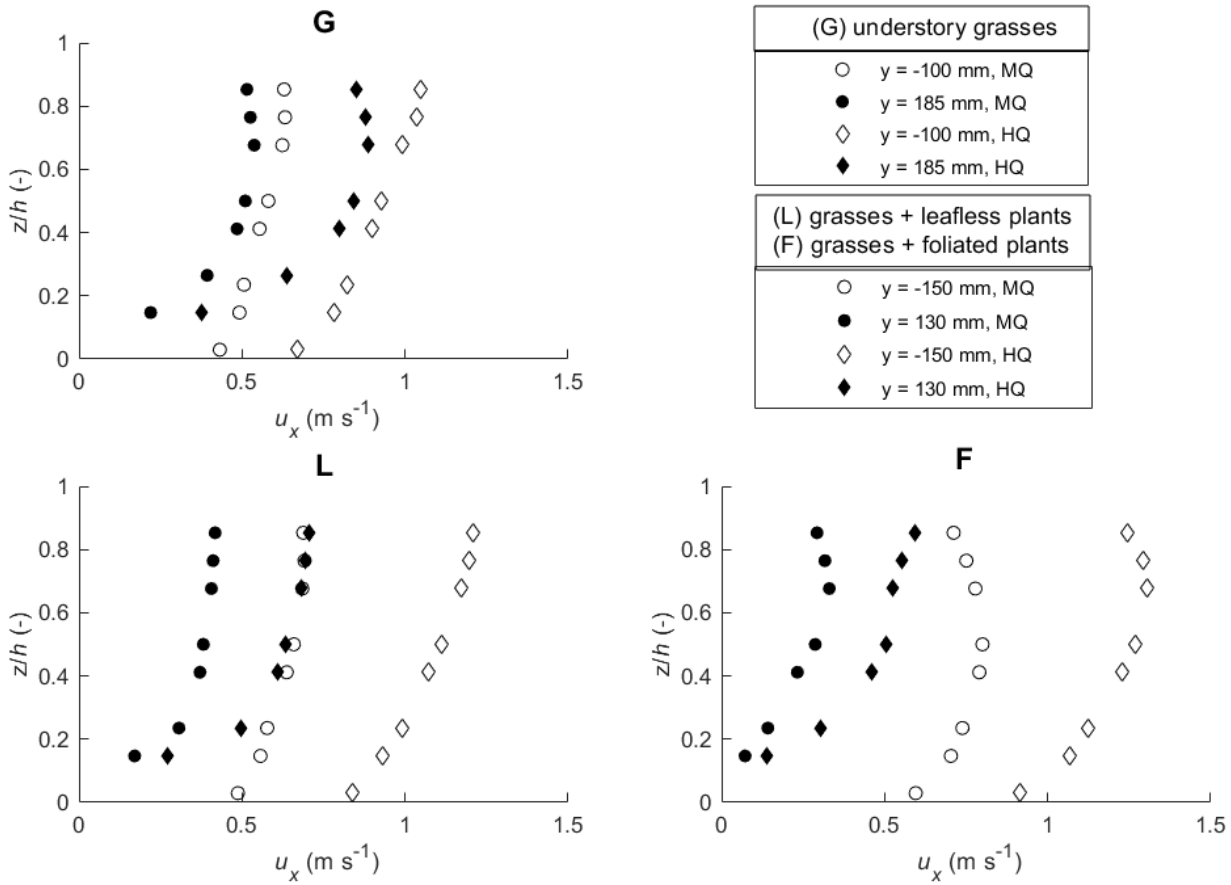

Figure 3. Vertical profiles of the streamwise flow velocity u_x for the six experimental conditions MQ-G & HQ-G (G), MQ-L & HQ-L (L) and MQ-F & HQ-F (F) representing the unvegetated channel part (y = -100 mm or y = -150 mm, open markers) and the vegetated channel part (y = 185 mm or y = 130 mm, filled markers) in the fully developed flow region at D = 7 m.

4.2 Vertical profiles of concentration

The time-averaged scaled concentration C_i ranged between 20 to 720 mg/l in the fully developed region of the flow at D = 7 m (Table 3). In general lower concentrations were observed in the vegetated areas of the flow. This is due to the reduction in streamwise flow velocity in the VP compared to the UP, despite the increase in turbulent intensities in the VP and near the interface regions. In the UP of the channel relatively high concentrations were observed near the bed (at z/h = 0.25). The highest concentrations (approx. 100-700 mg/l) were observed at the near bed in the UP in the HQ-L condition. In the UP the concentration was on average 1.5 to 2 times higher for the high-flow rate compared to the medium flow rate, while in the VP the concentration remained about equal. Extensive deposition of sediments in the vegetated areas limited longitudinal and lateral transport in the VP.

Table 3a. Scaled SSC, C_i (mg/l) for the point measurements taken over the vertical profile in the unvegetated part (y = -100 mm or y = -150 mm) of the channel for each tested experimental condition. Not measured or defined values are indicated as NA.

Vertical position	MQ-G	HQ-G	MQ-L	HQ-L	MQ-F	HQ-F
z/h (-)	C_i (mg/l)	C_i (mg/l)	C_i (mg/l)	C_i (mg/l)	C_i (mg/l)	C_i (mg/l)
0.85	NA	NA	70	100	54	66
0.75	60	94	73	103	54	69
0.70	60	88	74	116	56	84
0.50	62	81	72	137	58	96
0.40	65	83	88	200	75	123
0.25	75	99	135	285	107	167
0.15	88	101	211	718	210	293

Table 3b. Scaled SSC, C_i (mg/l) for the point measurements taken over the vertical profile in the vegetated part (y = 185 mm or y = 130 mm) of the channel, for each tested experimental condition. Not measured or defined values are indicated as NA.

Vertical position	MQ-G	HQ-G	MQ-L	HQ-L	MQ-F	HQ-F
z/h (-)	C_i (mg/l)	C_i (mg/l)	C_i (mg/l)	C_i (mg/l)	C_i (mg/l)	C_i (mg/l)
0.85	NA	NA	91	120	118	103
0.75	25	35	91	120	106	115
0.70	24	30	91	120	87	89
0.50	22	24	86	117	84	92
0.40	23	20	67	109	76	86
0.25	57	38	66	122	86	91

4.3 Sediment fluxes

Vertical profiles of sediment fluxes q_m at D = 7 m are shown in Figure 4, representing the UP (y = -100 mm or y = -150 mm) and VP (y = 185 mm or y = 130 mm) of the channel. This allow us to investigate the vertical variation in the sediment fluxes for the test conditions, and to point out differences in the profiles between the UP and VP of the channel. In the UP of the channel the q_m was considerably larger for positions near the bed compared to positions of larger flow depth. It is expected that the sediment fluxes were higher for positions closer to the near bed (z/h < 0.15) as the smooth bed resulted in relatively high near-bed flow velocities in comparison to the VP part of the channel. In the vegetative areas q_m is more uniformly distributed over the flow depth, and in the MQ-L, HQ-L, MQ-F and HQ-F conditions a small increase (10-15 mg $s^{-1}m^{-2}$) of q_m at the top of the water column (z/h > 0.7) was observed (Figure 4). The largest sediment flux q_m was observed at the measureable position located closest to the bed (at z/h = 0.15) in the UP for all the experimental conditions. The largest observed sediment flux was 93, 670 and 311 mg s^{-1} m^{-2} for the HQ-G, HQ-L, and HQ-F conditions respectively. In general, the highest suspended sediment fluxes were located where sediment concentration were highest. The sediment flux is expected to increase further in the unmeasured near bed-region (z < 0.15 h) due to the relative high near bed flow velocities (u_x > 0.5 m/s) just above the smooth bed. However, in natural conditions with rougher beds due to presence of e.g., dunes, cobbles and pebbles, woody debris or vegetation the sediment flux is expected to be limited by the low near bed flow velocities. As the result of a reduction in flow velocity and bed shear stresses in the localized areas caused by the macrotophography (Bouteiller and Venditti, 2015). This calls for future investigations of both the suspended and bed-load sediment fluxes in the near bed region of vegetated flows.

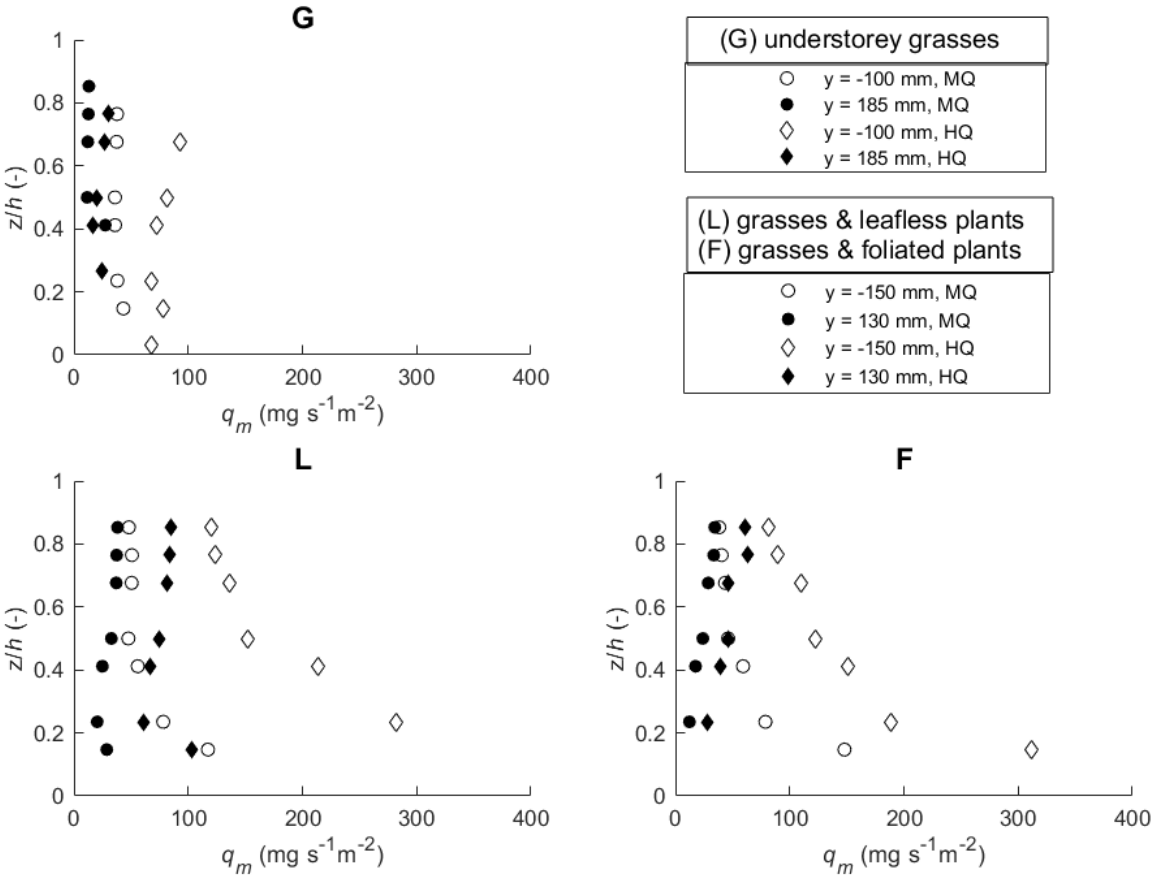

Figure 4. Vertical profiles showing the sediment fluxes q_m (mg s^{-1} m^{-2}) at D = 7 m for the tested experimental conditions MQ-G & HQ-G (G), MQ-L & HQ-L (L) and MQ-F & HQ-F (F) representing the unvegetated part (y = -100 mm or y = -150 mm, unfilled markers) and vegetated part (y = 185 mm or y = 130 mm, filled markers) of the channel.

4.4 Unit sediment discharges

The unit sediment discharge q_{tm} (discharge per unit width in g m-s^{-1}) at D = 7 m derived for the UP and VP for each of the tested conditions are shown in Table 4. The unit sediment discharge $q_{tm,UP}$ ranged between 4.6 and 32.1 g m-s^{-1} in the UP, and $q_{tm,VP}$ ranged between 1.5 and 9.0 g m-s^{-1} in the VP. The unit sediment discharges were 2 - 4 times higher in the UP at D = 7 m compared to the VP (Table 4). The largest difference was observed in the MQ-G conditions with relatively low streamwise flow velocities in the vegetative areas (Table 1). This resulted in extensive net deposition of particles that entered the vegetated areas from the unvegetated parts of the channel.

Table 4. Unit suspended sediment discharge $q_{tm,UP}$ and $q_{tm,VP}$ in the unvegetated and the vegetated part of the channel, respectively at D = 7 m, and ratio $q_{tm,VP}/q_{tm,UP}$.

Experimental condition	Unit SS discharge (UP) $q_{tm,UP}$ (g m-s^{-1})	Unit SS discharge (VP) $q_{tm,VP}$ (g m-s^{-1})	$q_{tm,VP}/q_{tm,UP}$ (-)
1. MQ-G	4.6	1.5	0.32
2. HQ-G	10	2.4	0.24
3. MQ-L	8.4	3.6	0.43
4. HQ-L	32.1	9.0	0.28
5. MQ-F	8.6	2.6	0.30
6. HQ-F	20.3	5.0	0.25

5 CONCLUSIONS

This study provided insight on the distribution on both the streamwise flow velocities and concentration with high temporal and spatial resolution for various vegetated conditions and bulk flow velocities. As expected, the depth-averaged streamwise flow velocity $\bar{u}$ were 1.5-3 times higher in the unvegetated parts of the channel compared to the vegetated parts (see Table 1). Larger velocity differences (up to 0.78 m/s) were observed for the foliated conditions compared to the leafless and grasses. This velocity difference, which relates to the strength of the shear layer is expected to be the main driver of lateral mixing of suspended sediment between the unvegetated and vegetated parts of the channel, and it determines the spatial distribution of the sediment fluxes.

The velocity and concentration profiles in the unvegetated parts resembled those expected for straight undisturbed channels with absence of vegetation. However, in the vegetative areas the concentration was more uniformly distributed over the flow depth. The unit sediment discharge was 2 to 4 times higher in the unvegetated part compared to the vegetated part of the channel (see Figure 4 and Table 4). Increase in bulk flow velocity caused a higher proportion of the sediments to be transported in the unvegetated part of the channel compared to the vegetated part (Table 4). Furthermore the presence of foliation increased the proportion of sediments transported in the unvegetated part, despite the increased lateral mixing of sediments. This can be explained by the enhancement of net deposition in the vegetative areas.

The findings in this study confirm that insight on the spatial variability of the mean flow velocities and concentration is important for accurate estimates of suspended sediment fluxes in vegetated flows. The results on the vertical and lateral distributions of the streamwise flow velocities, suspended sediment concentration profiles, and the sediment fluxes are useful for designing future experiments investigation flow-vegetation-sediment interactions. In particular, we expect to improve predictions of suspended sediment fluxes in natural partly vegetated channels.

ACKNOWLEDGEMENTS

The research reported herein is funded funded by Maa- ja vesitekniikan tuki ry (No 36537 and 33271) and by Maj and Tor Nessling Foundation (No 201800045). The authors would like to thank laboratory technician Antti Louhio for the help in the Aalto Environmental Hydraulics Lab, Gerardo Caroppi for the ADV data collection, and Markku Andelin for the help with the measurements and printing of the downscaled bed-load sampler.

REFERENCES

Aberle, J. and J. Järvelä, 2015. Hydrodynamics of Vegetated Channels. GeoPlanet: Earth and Planetary Sciences 1686:519–541.

Bouteiller, C. Le and J.G. Venditti, 2015. Sediment Transport and Shear Stress Partitioning in a Vegetated Flow. Water Resources Research:2901–2922.

Box, W., K. Västilä, and J. Järvelä, 2018. Transport and Deposition of Fine Sediment in a Channel Partly Covered by Flexible Vegetation. International Conference on Fluvial Hydraulics 40:02016.

Caroppi, G., K. Västilä, J. Järvelä, M. Rowi, and M. Giugni, 2019. Turbulence at Water-Vegetation Interface in Open Channel Flow: Experiments with Natural-like Plants. Advances in Water Resources 127:180–191.

Downing, J., 2006. Twenty-Five Years with OBS Sensors: The Good, the Bad, and the Ugly. Continental Shelf Research 26:2299–2318.

Druffel, L., W.W. Emmett, V.R. Schneider, and J. V Skinner, 1976. Laboratory Hydrualic Calibration of the Helley-Smith Bedload Sampler.

Dupuis, V., S. Proust, C. Berni, and A. Paquier, 2017. Mixing Layer Development in Compound Channel Flows with Submerged and Emergent Rigid Vegetation over the Floodplains. Experiments in Fluids 58:1–18.

Elliott, S.H., D.D. Tullos, and C. Walter, 2019. Physical Modeling of the Feedbacks between a Patch of Flexible Reed Canarygrass (Phalaris Arundinacea), Wake Hydraulics , and Downstream Deposition. Environmental Fluid Mechanics 19:255–277.

Gaudet, B.J.M., R.G. Andre, and J.L. Best, 1994. Effect of Orientation and Size of Helley-Smith Sampler on Its Efficiency. Journal of Hydraulic Engineering 120:758–766.

Hu, C., Z. Ji, and Q. Guo, 2010. Flow Movement and Sediment Transport in Compound Channels. Journal of Hydraulic Research 48:23–32.

Hu, Z., J. Lei, C. Liu, and H. Nepf, 2018. Wake Structure and Sediment Deposition behind Models of Submerged Vegetation with and without Flexible Leaves. Advances in Water Resources 118:28–38.

Jesson, M.A., J. Bridgeman, and M. Sterling, 2015. Advances in Engineering Software Novel Software Developments for the Automated Post-Processing of High Volumes of Velocity Time-Series. Advances in Engineering Software 89:36–42.

Julien, P.Y., 2010. Erosion and Sedimentation. Cambridge University Press.

Nepf, H.M., 2012. Flow and Transport in Regions with Aquatic Vegetation. Annual Review of Fluid Mechanics 44:123–142.

Nikora, V.I. and D.G. Goring, 2002. Fluctuations of Suspended Sediment Concentration and Turbulent Sediment Fluxes in an Open-Channel Flow. Journal of Hydraulic Engineering 128:214–224.

Ogston, A. and R. Stenberg, 1995. On the Importance of Nearbed Sediment Flux Measurements for Estimating

Sediment Transport in the Surf Zone. Continental Shelf Research 15:1061–1086.
Parsheh, M., F. Sotiropoulos, and F. Porté-Agel, 2010. Estimation of Power Spectra of Acoustic-Doppler Velocimetry Data Contaminated with Intermittent Spikes. Journal of Hydraulic Engineering 136:368–378.
Rowinski, M.P., K. Västilä, J. Aberle, J. Järvelä, and B.M. Kalinowska, 2018. How Vegetation Can Aid in Coping with River Management Challenges : A Brief Review. Ecohydrology & Hydrobiology:1–10.
Shah-Fairbank, S.C. and P.Y. Julien, 2016. Sediment Load Calculations from Point Measurements in Sand-Bed Rivers. International Journal of Sediment Research 30:1–12.
Tinoco, R.O. and G. Coco, 2018. Turbulence as the Main Driver of Resuspension in Oscillatory Flow Through Vegetation. Journal of Geophysical Research: Earth Surface:891–904.
Vargas-Luna, A., A. Crosato, G. Calvani, and W.S.J. Uijttewaal, 2016. Representing Plants as Rigid Cylinders in Experiments and Models. Advances in Water Resources 93:205–222.
Västilä, K. and J. Järvelä, 2018. Characterizing Natural Riparian Vegetation for Modeling of Flow and Suspended Sediment Transport. Journal of Soils and Sediments 18:3114–3130.
Yager, E.M. and M.W. Schmeeckle, 2013. The Influence of Vegetation on Turbulence and Bed Load Transport. Journal of Geophysical Research: Earth Surface 118:1585–1601.
Yang, J.Q. and H.M. Nepf, 2018. A Turbulence-Based Bed-Load Transport Model for Bare and Vegetated Channels. Geophysical Research Letters:428–436.
Zong, L. and H. Nepf, 2010. Flow and Deposition in and around a Finite Patch of Vegetation. Geomorphology 116:363–372.
Zong, L. and H. Nepf, 2011. Spatial Distribution of Deposition within a Patch of Vegetation. Water Resources Research 47:1–12.